



## Article

# Horizontal UHS Amplitudes for Regions with Deep Soil Atop Deep Geological Sediments—An Example of Osijek, Croatia

Borko Đ. Bulajić <sup>1</sup> , Marijana Hadzima-Nyarko <sup>2,\*</sup>  and Gordana Pavić <sup>2</sup>

<sup>1</sup> Faculty of Technical Sciences, University of Novi Sad, Trg Dositeja Obradovića 6, 21000 Novi Sad, Serbia; borkobulajic@yahoo.com

<sup>2</sup> Faculty of Civil Engineering and Architecture Osijek, Josip Juraj Strossmayer University of Osijek, Vladimira Preloga 3, 31000 Osijek, Croatia; gordana.pavic2@gmail.com

\* Correspondence: mhadzima@gfos.hr

**Abstract:** In this paper, we demonstrate how UHS-based seismic microzonation can be applied in low-to-medium seismicity areas with deep local soil and deep geological deposits under the local soil. The case study area surrounds the city of Osijek, Croatia, which is in the south-central region of the Pannonian Basin. New frequency-dependent scaling equations are derived, and the empirical response spectra are compared to the spectra of real strong motions in the surrounding region. Empirical calculations for deep soil atop deep geological strata show a 37% reduction in short-period spectral amplitudes when compared to rock locations. This demonstrates that local soil amplification is mitigated by energy dissipation in deep soils. For vibration periods longer than 0.3 s, spectral amplitudes are being amplified. This amplification goes up to 2.37 times for vibration periods around 0.5 s. UHS spectra for Osijek are computed using regional seismicity estimates, data on local soil and deeper geological surroundings, and newly created regional empirical equations for scaling various spectral amplitudes. UHS amplitudes for Osijek are also compared to the Eurocode 8 spectra for ground type C. The results show that ratios of the maximum UHS amplitudes to PGA values are up to 46% larger than the corresponding 2.5 factor that is recommended by Eurocode 8 for horizontal spectra. The UHS results might be viewed as preliminary for Osijek and regions with similar seismicity and local soil and deep geology conditions. When the number of regional strong-motion records grows many times beyond what it is currently, it will be feasible to properly calibrate the scaling equations, resulting in more reliable and long-term UHS estimations for the area under consideration.

**Keywords:** UHS; microzonation; scaling equations; deep local soil; deep geological deposits; Eurocode 8



**Citation:** Bulajić, B.Đ.; Hadzima-Nyarko, M.; Pavić, G. Horizontal UHS Amplitudes for Regions with Deep Soil Atop Deep Geological Sediments—An Example of Osijek, Croatia. *Appl. Sci.* **2021**, *11*, 6296. <https://doi.org/10.3390/app11146296>

Academic Editor: Antonio Cavallaro

Received: 18 June 2021

Accepted: 6 July 2021

Published: 7 July 2021

**Publisher's Note:** MDPI stays neutral with regard to jurisdictional claims in published maps and institutional affiliations.



**Copyright:** © 2021 by the authors. Licensee MDPI, Basel, Switzerland. This article is an open access article distributed under the terms and conditions of the Creative Commons Attribution (CC BY) license (<https://creativecommons.org/licenses/by/4.0/>).

## 1. Introduction

The amplification of ground motion generated by sedimentary basins has been investigated by many researchers using analytical and computational methods (e.g., [1–6]). However, standard seismic hazard maps only consider shallow geology conditions (i.e., the local soil conditions for the first 30 m depth of the stratigraphic profile). This is because most empirical equations for scaling peak ground acceleration (hereinafter, PGA) values only include the effects of local soil on a tens-of-meters scale and disregard the impact of deeper geological site conditions [7]. This is still the case, although there are studies that show that site resonance has little to do with the average shear-wave velocity of the upper 20 or 30 m [8]. Moreover, a series of recent seismic microzonation studies in the north-western Balkans [9–14] revealed that deep geology conditions have a significant impact on the severity of both short- and long-period waves. Here, the term “deep geology” is used to describe the geological conditions that characterize sites on a scale of hundreds of meters or kilometers [15].

The 2004 version of Eurocode 8 [16] recognizes the potential importance of deeper geological site surroundings, stating in Clause 3.1.2(1) that the National Annex may establish the classification scheme that will account for deep geology. However, to date, no EU country, including Croatia, has included deep geology into the ground classification scheme.

This study relies on our prior research [17,18] on the severity of surface ground motion in the case study area of Osijek, Croatia, and is accompanied by a study of vertical spectra [19]. Osijek is once again used as the case study area for low-to-medium seismicity regions and with deep soils atop deep geological sediments. In our study of the horizontal PGA values [17], we have shown that deep soil atop deep geological sediments leads to the de-amplification of seismic waves and ~17% lower PGA values than the values obtained at the rock sites. The subject of this particular paper will be the horizontal pseudo-absolute acceleration spectra (hereinafter, *PSA*).

Table 1 shows the ground types defined by the shear-wave velocity for the top 30 m of the soil profile,  $V_{S,30}$ , and corresponding maximum spectral accelerations, as defined by Eurocode 8 [16]. Official seismic hazard maps in Croatia are incorporated in the Croatian National Annex to Eurocode 8 [20]. The hazard is expressed by the PGA values for ground type A,  $a_g$  (see Table 1), i.e., for the rock sites [16]. As can be seen in Table 1, the maximum spectral amplitudes are equal to the product of  $a_g$ , 2.5 (a constant value for horizontal spectra), and the so-called soil factor [16], which is larger than 1 for all ground types. The fact that the soil factor is always larger than 1 indicates that there is an amplification of seismic waves regardless of the soil type. However, the empirical attenuation equations developed in the mid-1980s based on 1482 acceleration components from earthquakes in the western United States indicate that deep soil sites will lead to de-amplification of spectral amplitudes for vibration periods shorter than 0.4 s [21]. Cipta et al. [22] have recently studied the effects of site amplification and basin resonance in Jakarta, Indonesia. For short vibration periods (less than 1 s), they found that the levels of response spectral acceleration were significantly below those of the 2012 Indonesian building Codes' design response spectra, but approach or even exceed Code levels for longer periods [22]. They also discovered that available ground-motion prediction equations (hereinafter, *GMPE*) are incapable of capturing the impacts of basin geometry on seismic waves in a very deep basin filled with soft sediment [22].

**Table 1.** Maximum amplitudes of horizontal pseudo-absolute acceleration spectra *PSA* and corresponding vibration periods, *T*, for different ground types according to Eurocode 8 [16];  $a_g$  represents the horizontal PGA value obtained from the accompanying seismic hazard map.

Eurocode 8 [16] Ground Types	Type 1 Spectrum: "Most Contributing" Earthquakes with $MS > 5.5$	Type 2 Spectrum: "Most Contributing" Earthquakes with $MS \leq 5.5$
Ground type A, $V_{S,30} > 800$ m/s Rock, at the surface up to 5 m of weaker material.	$a_g \times 2.5$ $0.15 \text{ s} \leq T \leq 0.40 \text{ s}$	$a_g \times 2.5$ $0.05 \text{ s} \leq T \leq 0.25 \text{ s}$
Ground type B, $V_{S,30} = 360\text{--}800$ m/s At least several tens of meters thick deposits. Very dense sand, gravel, or very stiff clay.	$a_g \times 1.2 \times 2.5$ $0.15 \text{ s} \leq T \leq 0.50 \text{ s}$	$a_g \times 1.35 \times 2.5$ $0.05 \text{ s} \leq T \leq 0.25 \text{ s}$
Ground type C, $V_{S,30} = 180\text{--}360$ m/s Deep deposits, several tens of meters up to hundreds of meters thick. Dense or medium dense sand, gravel, or stiff clay.	$a_g \times 1.15 \times 2.5$ $0.20 \text{ s} \leq T \leq 0.60 \text{ s}$	$a_g \times 1.5 \times 2.5$ $0.10 \text{ s} \leq T \leq 0.25 \text{ s}$
Ground type D, $V_{S,30} < 180$ m/s Deposits. Loose-to-medium cohesionless soil or predominantly soft-to-firm cohesive soil.	$a_g \times 1.35 \times 2.5$ $0.20 \text{ s} \leq T \leq 0.80 \text{ s}$	$a_g \times 1.8 \times 2.5$ $0.10 \text{ s} \leq T \leq 0.30 \text{ s}$
Ground type E Alluvium layer at the surface, between 5 and 20 m thick, above stiffer material. $V_{S,30} < 360$ m/s.	$a_g \times 1.4 \times 2.5$ $0.15 \text{ s} \leq T \leq 0.50 \text{ s}$	$a_g \times 1.6 \times 2.5$ $0.05 \text{ s} \leq T \leq 0.25 \text{ s}$

The primary goal of this study is to assess the amplification (or de-amplification) effects of deep soil atop deep geological sediments on various spectral amplitudes and the incorporation of these effects into regional GMPEs. Local soil is classified according to Seed et al. [23,24], taking into account depths of more than 30 m. Hence, the term “deep soil” will be used to describe sites where the thickness of the soil layer overlying the layer with  $V_{S,30} > 800$  m/s is larger than 100 m.

Another goal of this research is to see if the spectral acceleration factor of 2.5 (i.e., the ratio between maximum spectral amplitudes and PGA values), as indicated by Eurocode 8, offers reasonable estimates for maximum spectral amplitudes.

This paper begins by outlining regional seismicity and site conditions in Osijek. It then goes on to present new regional empirical formulae for horizontal PSA prediction. Finally, uniform hazard spectra for a site in Osijek are created and compared to Eurocode 8 spectra. In addition, seismic hazard maps for several vibration periods and probabilities of exceedance are constructed.

## 2. Regional Seismicity and Local Site Conditions

The largest historical earthquake near Osijek, according to the SHARE European Earthquake Catalogue [25], happened on November 24, 1922. It had a magnitude of  $M_w = 4.6$ , an epicenter 20 km north of Osijek (see Figures 1 and 2), and a hypocentral depth of 18 km. The intensity in the epicentral region was VII–VIII (°MCS) and around VII (°MCS) in Osijek. Figure 1 depicts the epicenters of all  $M_w \geq 3$  earthquakes in the region from 1900 to April 2021 [26], as well as two recent devastating earthquakes in Croatia and the greatest historical earthquake near Osijek. The investigated area around Osijek is shown by the blue rectangle. As demonstrated in Figure 2, seismic activity in the studied area is less intense than in other parts of Croatia and the north-western Balkans.

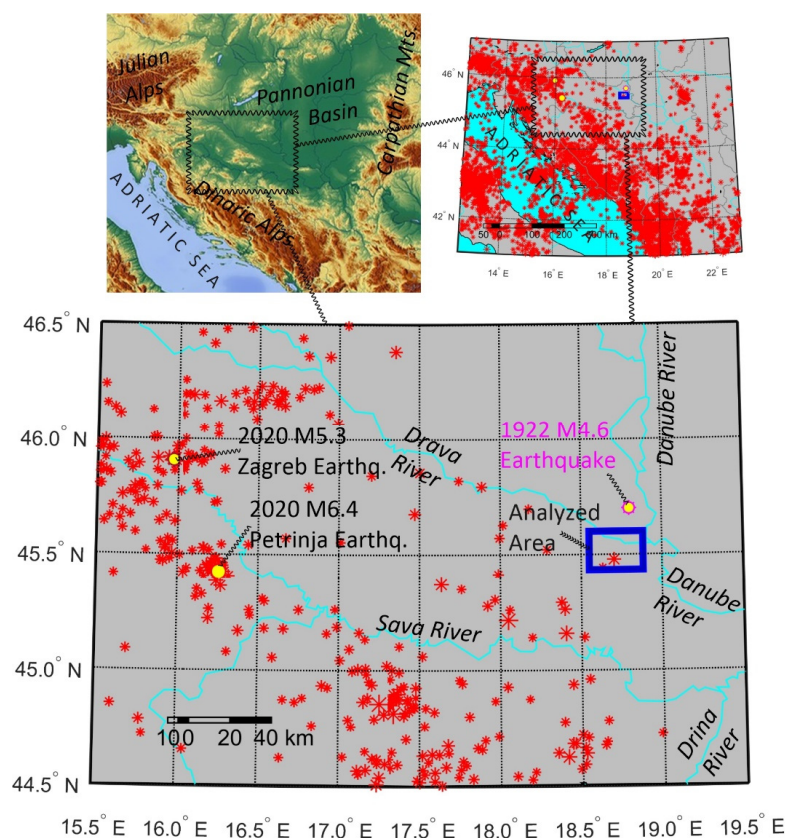


**Figure 1.** (Top left)—Pannonian Basin, (top right)—epicenters of regional earthquakes with  $M_w \geq 3$  [26], (bottom)—analyzed area and the epicenters of two recent destructive earthquakes and the largest historical earthquake closest to Osijek.

The city of Osijek is situated at the Pannonian Basin's southern end. Osijek is located on the right bank of the Drava River, and the local soil layers consist of muddy and sandy soil with elevated groundwater levels. According to Seed's classification [23,24], the local soil is deep soil, with a total thickness of 150–180 m above layers with an s-wave velocity greater than 800 m/s [27]. According to Eurocode 8 [16], local soil is of ground type C, as shear-wave velocity is between 180 and 360 m/s in the top 30 m. The deep geological formations underneath Osijek have depths ranging from 1.2 to 2.7 km and represent a combination of marls, sandstones, conglomerates, and limestones [27], dating back to the Pannonian Sea. According to the deep geology categorization by Trifunac and Brady [15], these deposits can be classified as geological sediments.

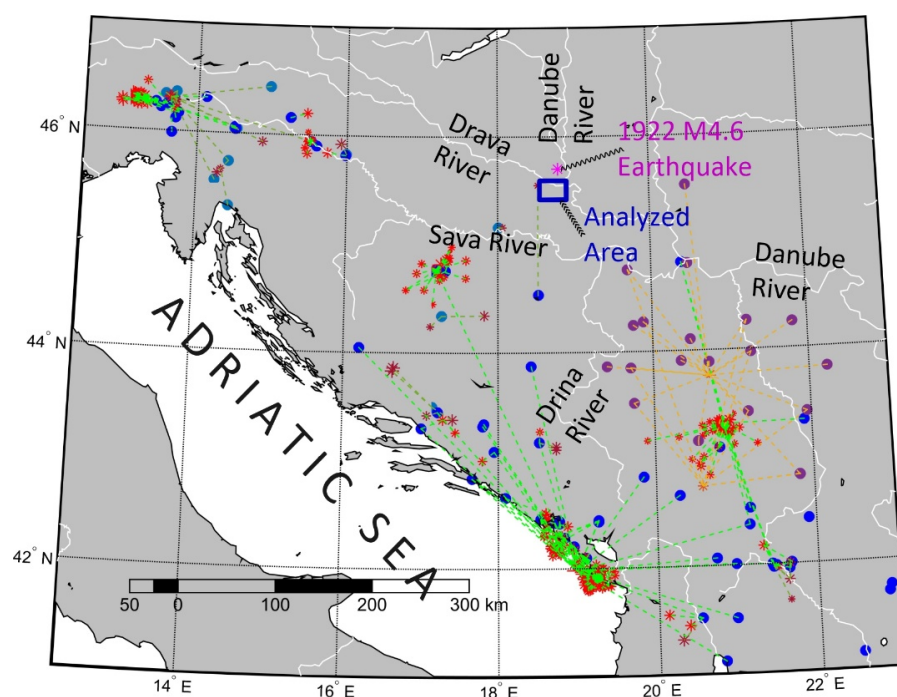


**Figure 2.** Analyzed area and the regional strong-motion data. Blue circles and red asterisks represent the recording sites and earthquake epicenters for the accelerograms in the EQINFOS [28] and IESD [29,30] databases, respectively. Green dashed lines connect the epicenters to the recording stations. Violet circles and orange asterisks indicate the locations of the recording sites and earthquake epicenters for the accelerograms provided by Seismological Survey of Serbia [31].

### 3. Empirical Scaling Equations vs. Real Records

In this study, we generate new empirical equations for predicting  $PSA$  values that can be applied to deep soil sites atop deep geological strata. We utilize the same approach as Bulajić et al. [17–19], and the GMPE for the horizontal direction is written in the following mathematical form:

$$\log[PSA(T)] = c_1(T) + c_2(T) \cdot M + c_3(T) \cdot \log(\sqrt{R^2 + R_0(T)^2}) + c_4(T) \cdot S_{L1} + c_5(T) \cdot S_{L2} + c_6(T) \cdot S_{G1} + c_7(T) \cdot S_{G2} + \sigma_{\log}(T) \cdot P \quad (1)$$

where  $PSA(T)$  stands for horizontal pseudo-absolute acceleration spectra (in [g]) for vibration periods  $T$ ,  $M$  for earthquake magnitude, and  $R$  for either hypocentral or epicentral distance in kilometers (we develop equations for each type of distance).  $S_{L1}$  and  $S_{L2}$  are categorical variables for local soil (shallow geology) conditions, and  $S_{G1}$  and  $S_{G2}$  are categorical variables for deep geological conditions. Table 2 shows the values of these variables. According to [23,24], the local soil is divided into three types: “rock” soil sites, stiff soil sites, and deep soil sites. According to [15], deep geology is separated into three categories:



geological rock, deep geological sediments, and intermediate (or complex) geological site surroundings. Furthermore, the data were assumed to have a log-normal distribution. In Equation (1),  $\sigma_{log}$  is the standard deviation of the common logarithm of  $PSA$ , where  $\varepsilon$  is 0 is the median estimate and 1 for the median + 1  $\sigma_{log}$  estimate.

**Table 2.** The categorical variables employed in this study’s scaling equations for various types of shallow and deep geological site surroundings.

Shallow Geology Categorical Variables	Shallow Geology Type	Deep Geology Categorical Variables	Deep Geology Type
$S_{L1} = S_{L2} = 0$	“Rock” soil: $s_L = 0$	$S_{G1} = S_{G2} = 0$	Basement (geological) rock: $s = 2$
$S_{L1} = 1$ and $S_{L2} = 0$	Stiff soil: $s_L = 1$	$S_{G1} = 1$ and $S_{G2} = 0$	Intermediate sites: $s = 1$
$S_{L1} = 0$ and $S_{L2} = 1$	Deep soil: $s_L = 2$	$S_{G1} = 0$ and $S_{G2} = 1$	Deep geological sediments: $s = 0$

A map of the regional strong-motion data available to the authors is shown in Figure 2. The recording sites and earthquake epicenters for the accelerograms in the EQINFOS [28] and ISED [29,30] databases are represented by blue circles and red asterisks, respectively. The locations of the recording sites and earthquake epicenters for the strong-motion accelerograms provided by Seismological Survey of Serbia [31] are indicated by violet circles and orange asterisks, respectively. It should be noted that the north-western Balkans is one of the few regions on the planet where data on deep geological site conditions are accessible for many recording stations. Moreover, ground motion predictions based on scaling equations that simultaneously consider local soil conditions (up to depths of 100 m and more) and deep geology have shown to be in excellent agreement with recorded ground motions and observed intensities in the region [32,33].

The strong-motion database used to create predictive equations contains 436 horizontal components of strong-motion accelerograms recorded in the north-western Balkans from 112 earthquakes with magnitudes between 3 and 6.8. The majority (418) occurred between 1976 and 1987, with the remainder (18) occurring in 2010. The majority of contributing earthquakes were shallow with focal depths of less than 10 km. The majority of accelerograms were recorded at epicentral distances of less than 100 km, while the fault distance data for many of the accelerograms were either unavailable or unreliable. As a result, we used either epicentral or hypocentral distance for empirical prediction equations. More information on this database can be found in Bulajić et al. [17].

In two phases, we ran multiple linear regression analyses. The relevant MATLAB® scripts for deriving the scaling coefficients were prepared in MATLAB® version 8.5, release 2015a. In the first phase, we fitted the Equation (1) model to a dataset containing only the 406 horizontal acceleration components from the EQINFOS database [28]. We fitted Equation (1) without the coefficient  $c_5$  because there were no deep soil locations among the 406 components. As a result, we only calculated coefficients  $c_1$ ,  $c_2$ ,  $c_3$ ,  $c_4$ ,  $c_6$ , and  $c_7$ . To maximize the  $R^2$  statistics of the  $PSA$  prediction, the  $R_0$  values were iteratively changed. Because most of the data were collected at shorter distances, we conducted a secondary analysis utilizing only data collected at epicentral distances of less than 30 km. We calibrated the generated prediction model in the second phase by restricting the coefficient  $c_5$  (again through linear regression) based on the extra 30 acceleration components recorded at 10 different deep soil sites in the analyzed region. Table A1 (see Appendix A) gives coefficients for Equation (1) with  $R$  as the epicentral distance based on the data collected at all distances. Table A2 shows the scaling coefficients for Equation (1) with  $R$  as the hypocentral distance.

Attenuation of  $PSA(T)$  with distance is shown in Figures 3 and 4 for four distinct vibration periods,  $T = 0.05, 0.10, 0.30$ , and  $0.50$  s. Figure 3 presents empirical forecasts

for three different deep geology types at deep soil sites ( $s_L = 2$ ). The solid lines represent median empirical estimates based on data recorded at all epicentral distances, whereas the dashed lines represent estimates based on distances under 30 km. Figure 4 presents empirical predictions for three different local soil types at deep geological deposits ( $s = 0$ ). In Figure 4, we show the median, median  $\pm 1 \sigma_{log}$ , and median  $\pm 2 \sigma_{log}$  (shaded area) empirical estimates for the deep soil sites.

The coefficients corresponding to the categorical variables  $S_L$  and  $S_G$  can be used to calculate the exact differences between values estimated for different site conditions. For example, if the coefficients from Table A1 are used, the  $PSA$  (0.05 s) estimates (which can be considered as the upper bound for  $PGA$  estimates) are  $1/10^{-0.143} = 1.39$  times larger at the geological rock ( $s = 2$ ) than at the deep geological sediments ( $s = 0$ ), as seen in the top left-hand side plot in Figure 3. This is most likely because short-period waves travel more easily through more compact rocks (e.g., granites and basalts). Conversely, the  $PSA$  (0.50 s) estimates are  $10^{0.137} = 1.37$  times larger at the sediments than at the geological rock, as seen in the bottom right-hand side plot in Figure 3.

Furthermore, by using coefficients from the same Table A1, the  $PSA$  (0.05 s) at deep soil sites is going to be equal to  $10^{-0.058} = 0.88$  times the  $PSA$  (0.05 s) for rock soil sites. In other words, the seismic waves will be de-amplified, as shown in the top left-hand side plot in Figure 4. This suggests that energy dissipation in deep soil overcomes local soil amplification, which is consistent with the findings of numerous other research studies of the non-linear behavior of soft sediments under significant ground motion. However, for larger vibration periods, there is no de-amplification. For example, as shown in the bottom right-hand side plot in Figure 4, the  $PSA$  (0.50s) at deep soil sites is going to be  $10^{0.238} = 1.73$  times larger than the value for rock soil sites.

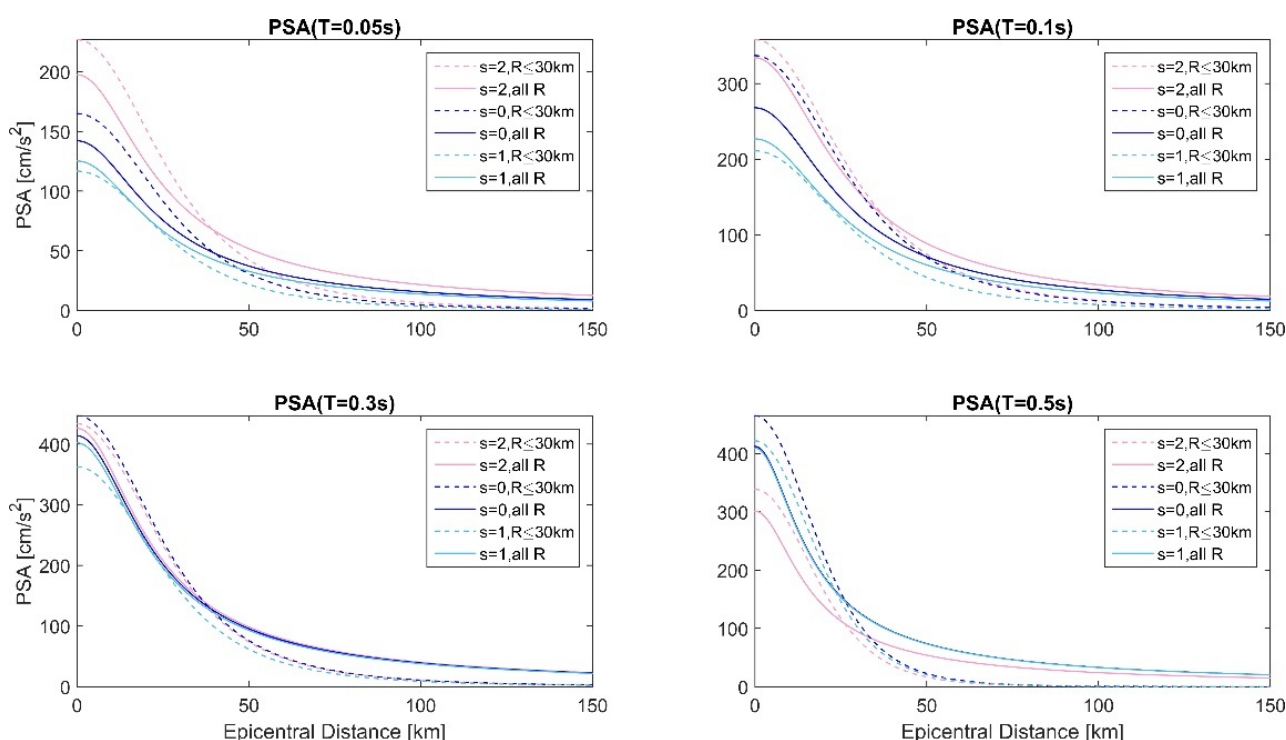


**Figure 3.** Empirical GMPE for four different vibration periods,  $T = 0.05, 0.10, 0.30$ , and  $0.50$  s, calculated using Equation (1) and coefficients from Table A1, for deep soil sites ( $s_L = 2$ ) and for different deep geology parameters ( $s = 2$  for geological rock sites,  $s = 1$  for intermediate geological surroundings, and  $s = 0$  for geological sediments). The solid lines represent median empirical predictions based on coefficients created for all source-to-site distances, whereas the dashed lines represent predictions based on coefficients developed for distances less than 30 km.

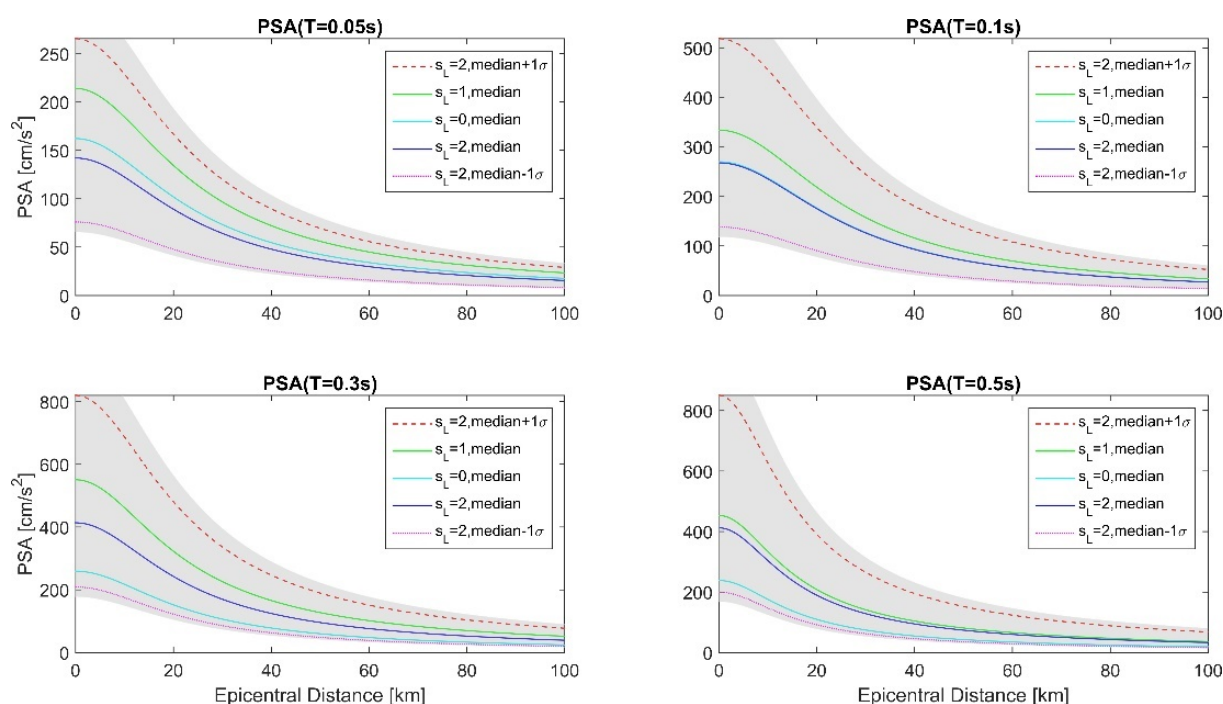


**Figure 4.** Median, median  $\pm 1 \sigma_{\log}$ , and median  $\pm 2 \sigma_{\log}$  (shaded area) empirical PSA estimates for the deep soil sites ( $s_L = 2$ ), and median estimates for rock soil ( $s_L = 0$ ) and stiff soil ( $s_L = 1$ ) sites.

The coupled effect of deep soils and deep geological sediments can be assessed by considering both  $c_5$  and  $c_7$  from Tables A1 and A2. For example,  $PSA(0.05\text{ s})$  at deep soil atop deep geological sediments will be  $10^{-0.058} \cdot 10^{-0.143} = 0.63$  of the value for rock soil atop the geological rock when coefficients from Table A1 are considered. This indicates even larger de-amplification than when only deep soil effects (i.e., only  $c_5$ ) are analyzed. On the other hand, the amplification of  $PSA$  amplitudes will occur for vibration periods between  $\sim 0.3\text{ s}$  and  $\sim 1\text{ s}$ . For  $PSA(0.50\text{ s})$ , the amplification for deep soil atop deep geological sediments will be equal to  $10^{0.238} \cdot 10^{0.136} = 2.37$ .

The only GMPEs we can compare our results to (as they also simultaneously consider effects of deep soils and deep geological sediments) are the ones developed for California based on 1482 strong-motion records from earthquakes in the western United States [21]. Moreover, the author of these GMPEs used the same categorical variables as we did (see Table 2) [21], and the site amplification can also be assessed simply by analyzing corresponding scaling coefficients. For the vibration period of  $T = 0.04\text{ s}$ , for example, Californian GMPEs indicate 30% lower  $PSA$  amplitudes at the deep soil atop deep geological sediments than at the rock sites, which is very similar to what we obtained for  $T = 0.05\text{ s}$ . Furthermore, according to the Californian GMPEs [21], the amplification exists for the vibration periods longer than  $0.3\text{ s}$ , and the maximum amplification is  $\sim 1.7$ , which is somewhat smaller than what we obtained.

The spectra of both orthogonal horizontal components of 15 accelerograms recorded at deep soil sites are compared in Figure 5 to the empirical predictions defined by Equation (1) and the scaling coefficients from Table A2. The actual and predicted spectra exhibit a great degree of agreement, as is shown.

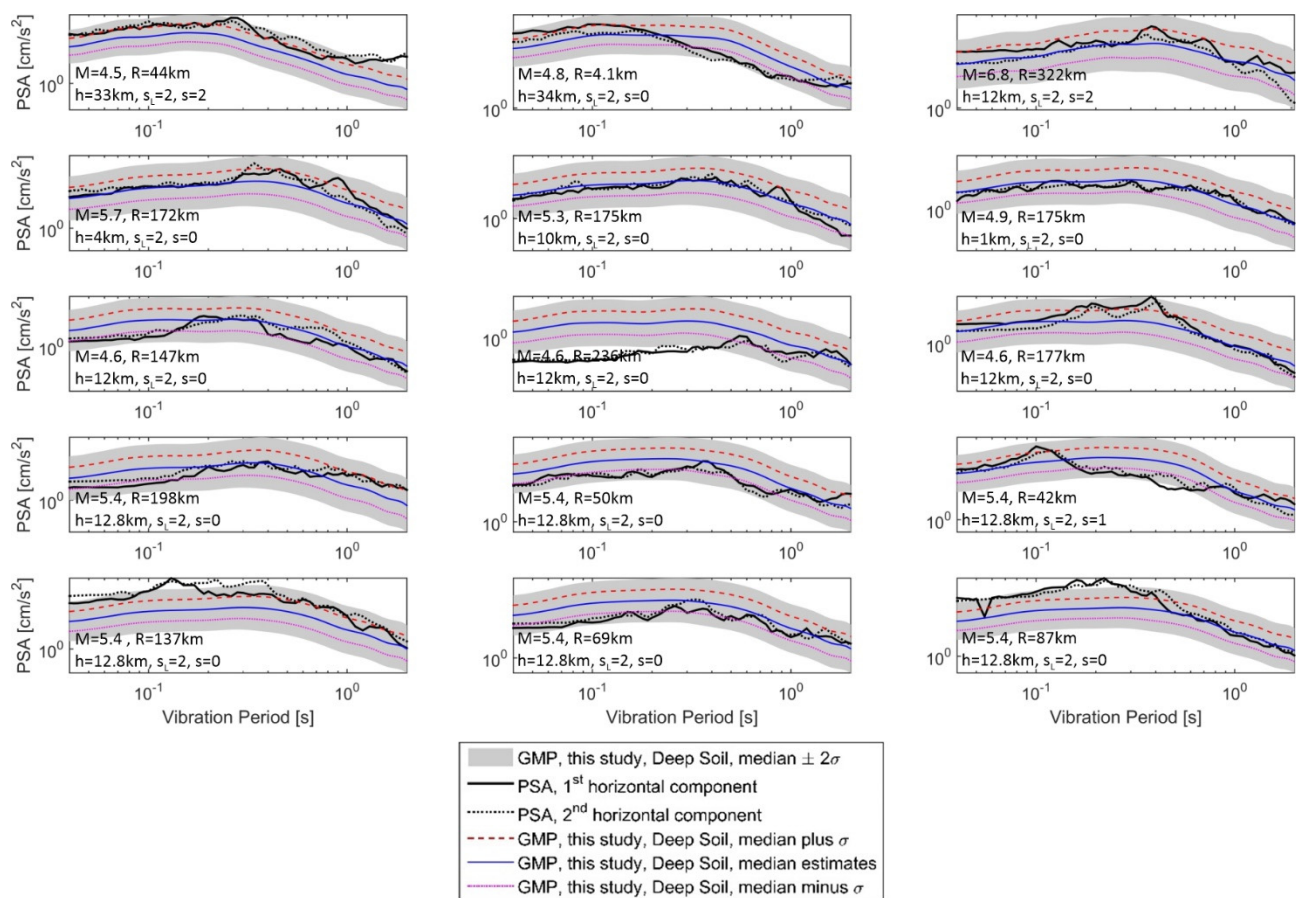


**Figure 5.** Correlation between regional horizontal pseudo-acceleration spectra recorded at deep soil sites ( $s_L = 2$ ) and the empirical predictions of Equation (1) and the coefficients in Table A2.

Several recent regional microzonation investigations [9–14] have also demonstrated that empirical predictions based on scaling equations that take into consideration both the deep geology and local soil are in excellent agreement with recorded ground motions in the region. Therefore, despite the limitations of the used strong-motion data, we employ the scaling equation derived in this study for the probabilistic hazard analyses for Osijek, just as we did for vertical spectra [19]. It is easy to update the empirical scaling equations and redo the hazard estimations as the number of acceleration records grows.

#### 4. Uniform Hazard Spectra and Seismic Hazard Maps for Osijek

In this section, we perform a probabilistic seismic hazard assessment (hereinafter, PSHA) analysis utilizing Equation (1) as the GMPE and coefficients from Table A1, assuming the deep soil sites and deep geological layers throughout the analyzed area. We also employ the SHARE Project's pan-European seismic source zone model [34–36]. The boundaries of the seismic source zones employed in this study's hazard calculations are depicted in Figure 6. The same figure also shows the radii of 123, 184, and 228 km, which show the epicentral distances that must be incorporated in the PSHA calculations for the 475-year return period to obtain 1% accuracy for computed spectral amplitudes at 0.05, 0.3, and 0.5 s, respectively. These radii show that the short-period spectral amplitudes are less sensitive to the occurrence of distant strong earthquakes and are dominated by the local seismic activity. Furthermore, the circle with a radius of 43 km designates the distances that contribute to 50% accuracy of PSHA calculations for the 0.5 s spectral amplitude. The epicenter of the largest historical (M 4.6, 1922) earthquake near Osijek, which is also shown in Figure 6, falls almost within this radius around the analyzed area.



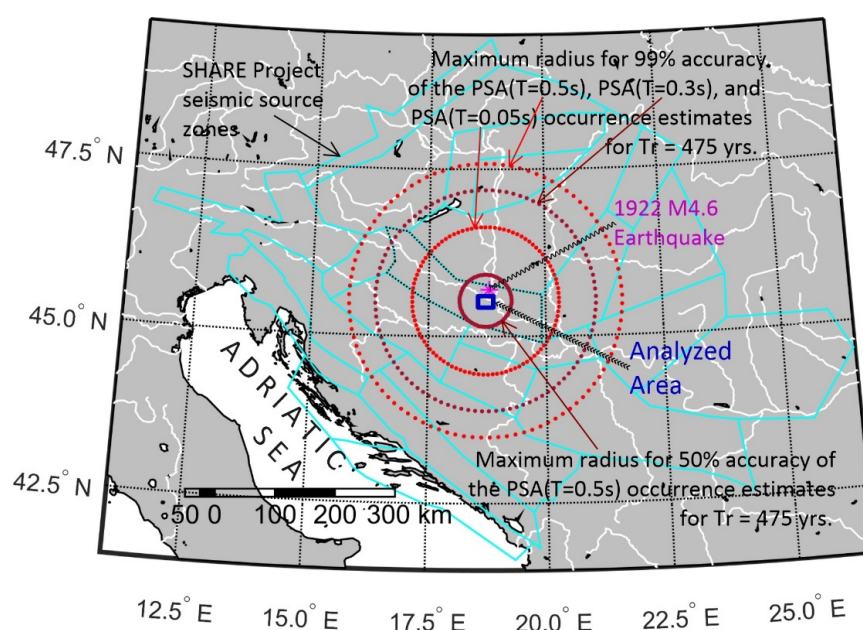


**Figure 6.** Boundaries of the seismic source zones used in the hazard calculations. Circles around the analyzed area show maximum radii for capturing 99% or 50% accuracy of the  $T_r = 475$  years PSA estimations for vibration periods of 0.05, 0.3, and 0.5 s.

The PSHA estimations were generated with REASSES V2.0 software [37], which is based on Cornell [38] and McGuire's [39] methodology. According to this methodology, to calculate the mean yearly rate of occurrence,  $N(a)$ , of seismic events that will cause a ground motion PSA amplitude " $A$ " to exceed expectation " $a$ ", products of probabilities related to distance, magnitude recurrence, and GMPE predictions are integrated over all the considered magnitudes and distances and summed. If homogeneous Poisson distribution is assumed, the probability of at least one yearly exceedance of the expectation  $a$  can be calculated as follows [40]:

$$P(a) = 1 - e^{-N(a)}. \quad (2)$$

If a binomial distribution is additionally considered, the chance that  $A$  will surpass  $a$  at least once throughout  $t$  years can be estimated as follows [40]:

$$p(a) = 1 - [1 - P(a)]^t \quad (3)$$

The so-called return period,  $T_r$ , is then equal to  $N(a)^{-1}$  and does not (in general) correlate to any single engineeringly significant earthquake. Magnitudes and distances of earthquakes contributing to  $N(a)$  can be determined using a technique known as "seismic hazard disaggregation" [41]. In the disaggregation, we can additionally define the values of the number of standard deviations that  $\log(a)$  is distant from the median empirical estimate for each pair of magnitude and distance [42].

Figure 7 shows hazard disaggregation examples for the coordinates  $45^\circ 32' \text{ N}$ ,  $18^\circ 23' \text{ E}$ . Top plots and the bottom-left plot in Figure 8 show cumulative disaggregation for distances and magnitudes. The magnitude recurrence curve for the most contributing seismic source zone surrounding Osijek is in the bottom-right plot. As can be observed, the real return periods of the most contributing earthquakes vary depending on the vibration period and are substantially shorter than the so-called return period  $T_r$ , defined as a reciprocal value of the mean yearly rate of occurrence,  $N(a)$ . This is significant because Eurocode 8 [16] does not define Types 1 and 2 spectra in terms of maximum credible earthquake magnitudes but rather in terms of magnitudes that "contribute most to the seismic hazard defined for the site for the purpose of probabilistic hazard assessment" (see Eurocode 8 [16]: 3.2.2.1, (4), Note 2 and 3.2.2.2, (2)P, Note 1).

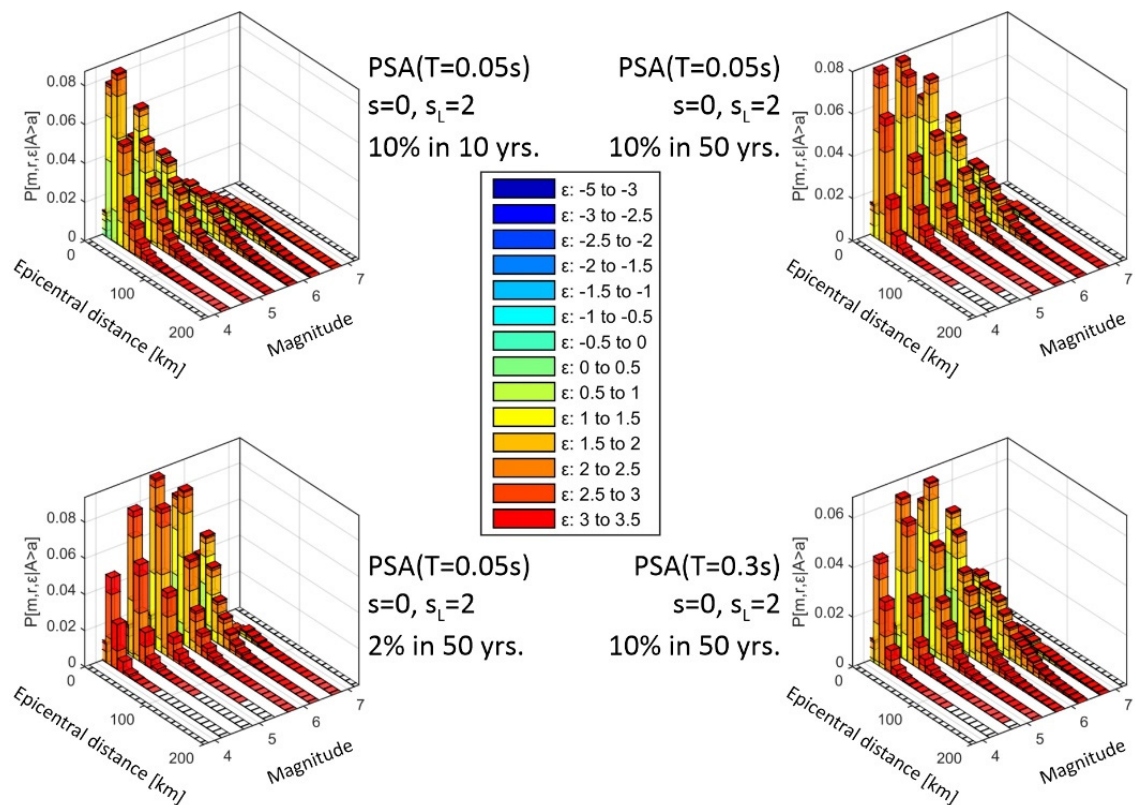


**Figure 7.** Examples of seismic hazard disaggregation for the location with coordinates 45°32' N, 18°23' E (see the full circles in Figure 9).

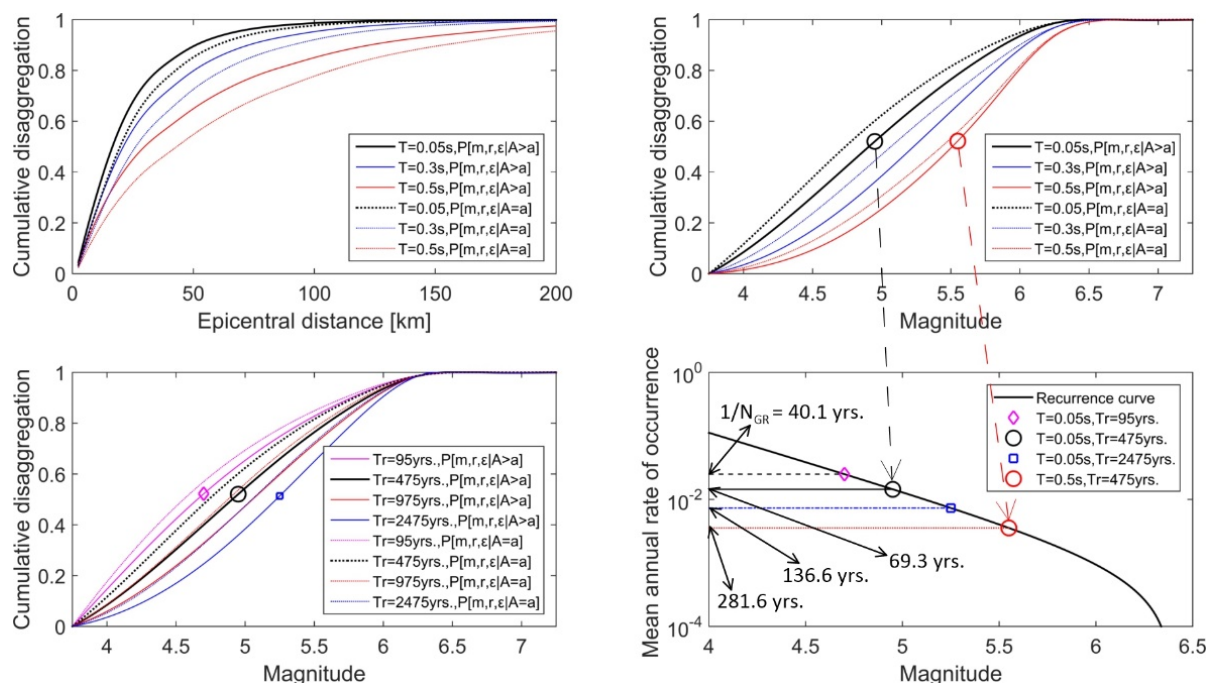


**Figure 8.** Cumulative disaggregation examples for distance and magnitude, and the magnitude recurrence curve for the most contributing seismic source zone around Osijek.

The seismic microzonation maps for the research area are depicted in Figure 9 for the return periods  $Tr$  of 95, 475, 975, and 2475 years. Finally, for the coordinates 45°32' N, 18°23' E, uniform hazard spectra were produced for four different probability levels and

compared to the Eurocode 8 [16] Type 2 spectra for ground type C. Figure 10 compares the resulting uniform hazard spectra (hereinafter, UHS) for several deep geology and local soil types to the Eurocode 8 spectra for ground type C, scaled by the PGA values at deep soil sites ( $s_L = 2$ ) and for three different deep geology types. As can be seen, the maximum UHS amplitudes to PGA ratios, referred to as  $S_{PGA}$  in Figure 10, deviate from the 2.5 factor indicated by Eurocode 8 [16] for horizontal spectra. The difference between  $S_{PGA}$  and the 2.5 factor slightly increases with the so-called return period. For the 475-year return period,  $S_{PGA}$  for deep soils atop deep geological sediments ( $s = 0$ ,  $s_L = 2$ ) will be 37% larger than the factor suggested by Eurocode [16]. For the 2475 years,  $S_{PGA}$  for the same site conditions will be 46% larger than 2.5. The differences are even larger if we consider UHS amplitudes for deep soils atop geological rocks ( $s = 0$ ,  $s_L = 2$ )— $S_{PGA}$  will be 60% larger for 475-year and 67% larger for 2475-year return periods. The only time when  $S_{PGA}$  is similar to 2.5 is when UHS is calculated for deep geological sediments and stiff soils ( $s = 0$ ,  $s_L = 1$ ). Here, “stiff soils” sites are those with a soil layer 15–75 m thick overlying the layer with  $V_{s,30} > 800$  m/s [23,24].

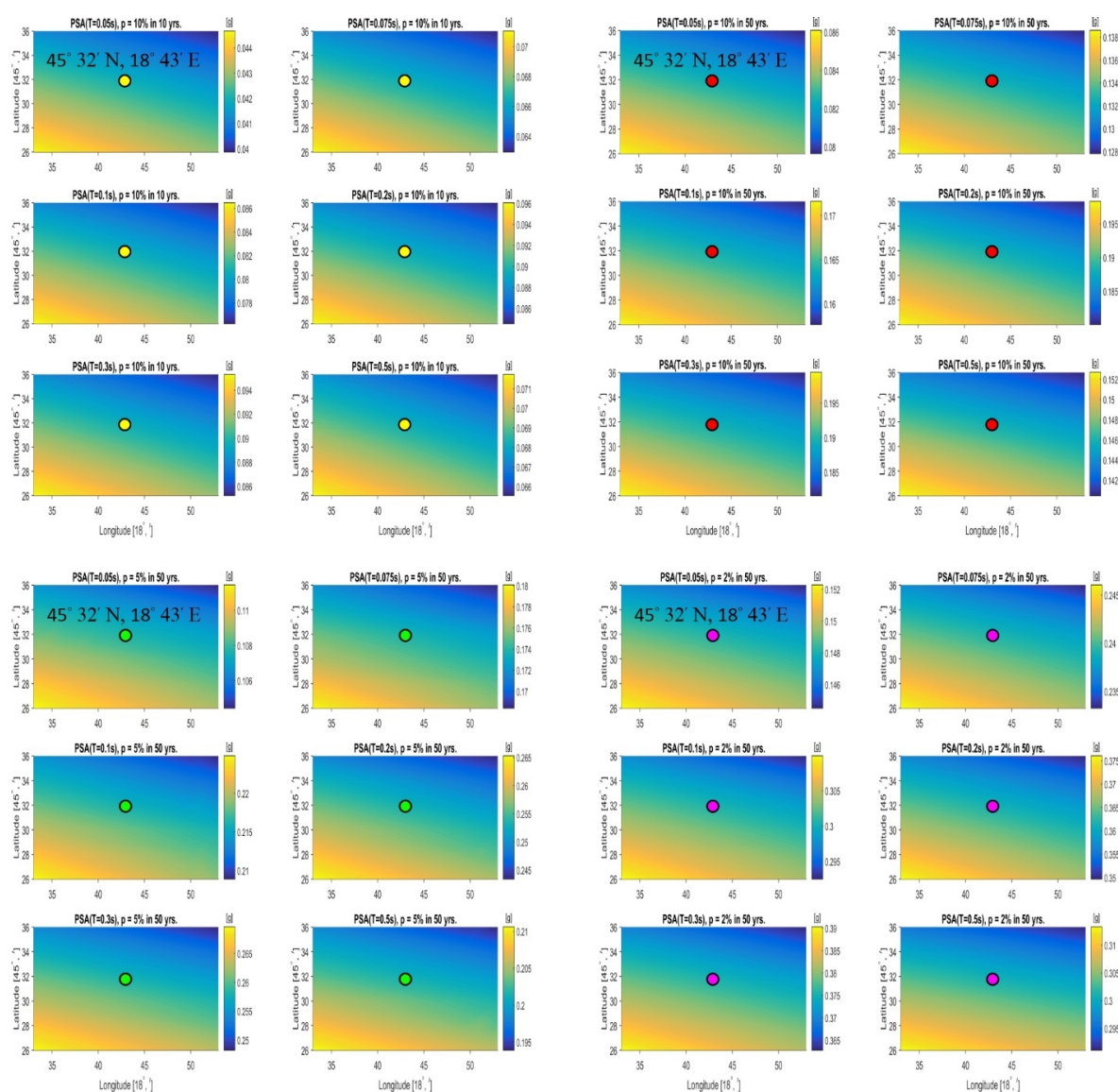


**Figure 9.** Seismic hazard maps for 6 different PSA amplitudes and probabilities of exceedance of 10% in 10 years (6 top-left plots), 10% in 50 years (6 top-right plots), 5% in 10 years (6 bottom-left plots), and 2% in 50 years (6 bottom-right plots). The site chosen for UHS and disaggregation calculations is shown by full circles.



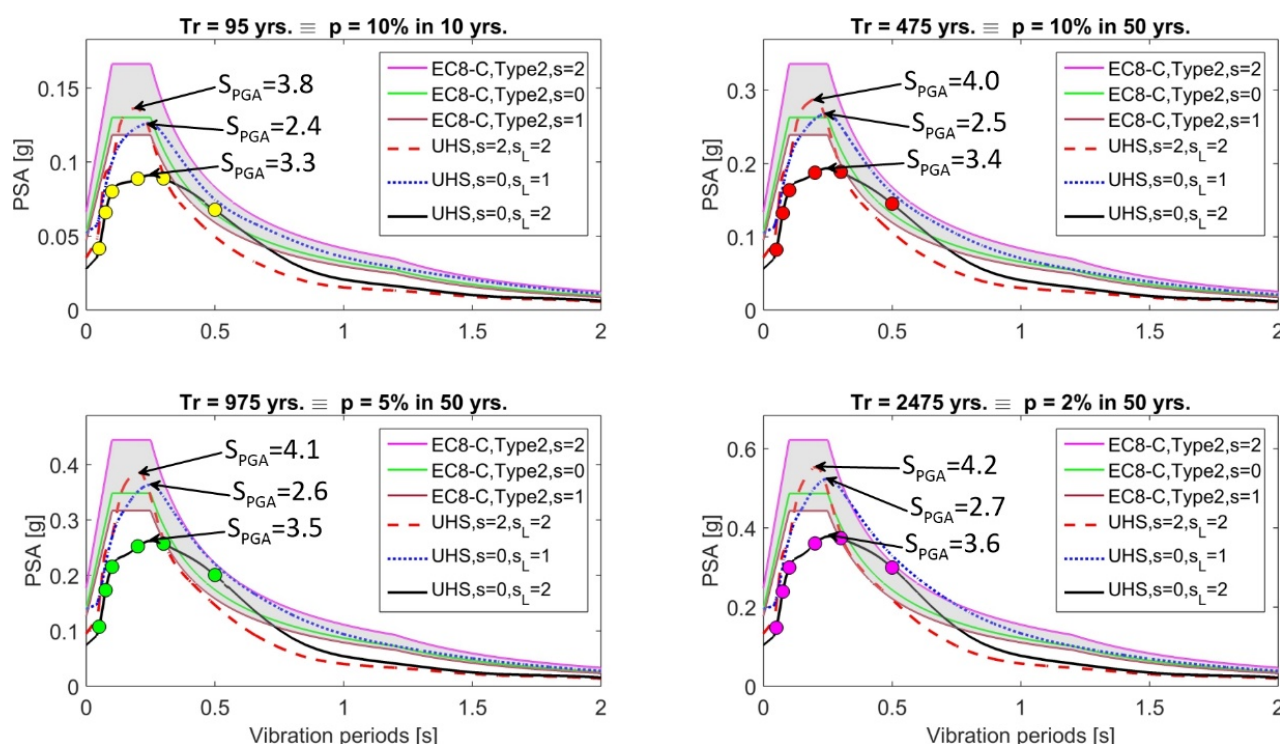


**Figure 10.** The uniform hazard spectra calculated for the coordinates  $45^{\circ}32' \text{ N}$ ,  $18^{\circ}23' \text{ E}$  for four different probability levels, and the Eurocode 8 [16] Type 2 spectra for ground type C.

## 5. Discussion and Conclusions

This research was motivated by recent seismic microzonation studies in the north-western Balkans region [9–14], which revealed that variations in deep geological site conditions can significantly increase seismic hazard estimates when compared to the hazard estimates based only on the effects of the local soil. At the same time, other recent studies indicated a high vulnerability of the city of Osijek's building stock [43,44].

In this study, we analyzed horizontal UHS estimates for deep soil sites atop deep geological sediments in low-to-medium seismicity areas. For the case study, we chose the city of Osijek, Croatia, located in the southern part of the Pannonian Basin and on the right bank of the Drava River. Geological sediments underneath Osijek have depths ranging up to 2.7 km, while the total thickness above layers with an s-wave velocity greater than 800 m/s is 150–180 m.

New empirical regional formulae for PSA attenuation were first developed based solely on the regional strong-motion data. The strong-motion database used to create predictive equations includes 436 horizontal components of strong strong-motion accelerograms recorded in the north-western Balkans from 112 earthquakes with magnitudes ranging from 3 to 6.8. The provided equations take into account the effects of local soil and deep geological conditions at the same time. According to empirical estimations, the combination of deep soil and deep geological deposits results in short-period spectral amplitudes up to 37% lower than those obtained at rock soil locations. This suggests that energy dissipation in deep soil sites overcomes local soil amplification, which is consistent with other recent studies of soft sediment non-linear behavior (e.g., [45,46]). Vice versa, spectral amplitudes for vibration periods  $T > \sim 0.3 \text{ s}$  are shown to be amplified. This is consistent with the findings of Bijelic et al. [47], who investigated the impact of deep basin effects on structure collapse and discovered that vibration periods longer than 1.2 s increased the chance of structural collapse by up to 20%. In this study, the maximum amplification of 2.37 times was obtained for  $T = 0.5 \text{ s}$ .

The only GMPEs to which we can compare our findings (since they consider effects of deep soils and deep geological sediments at the same time) are those created for California



based on 1482 strong-motion records from earthquakes in the western United States [21]. Californian GMPEs, for example, show 30% lower *PSA* amplitudes in the deep soil than in the rock sites for  $T = 0.04$  s. According to Californian GMPEs [21], the amplification exists for vibration intervals longer than 0.3 s, and the highest amplification is 1.7, which is a little lower than what we obtained.

Based on the presented scaling equations, UHS amplitudes were calculated for the analyzed area and the microzonation maps created. The resulting uniform hazard spectra were compared to the Eurocode 8 [16] spectra for ground type C, scaled by the PGA values at deep soil sites, and for three different types of deep geology. As can be observed in Figure 10, the ratios of the maximum UHS amplitudes to PGA values,  $S_{PGA}$ , diverge from the 2.5 factor recommended by Eurocode 8 for horizontal spectra. In the case of UHS amplitudes for deep soils atop deep geological sediments,  $S_{PGA}$  is equal to 3.3 for 95-year, 3.4 for 475-year, 3.5 for 975-year, and 3.6 for 2475-year return periods. This is a 31–46% increase compared to the 2.5 factor suggested by Eurocode 8.

Although the data used for the definition of the GMPEs used for hazard calculations are limited, we believe that the presented hazard maps and uniform hazard spectra can be seen as the first step towards more reliable hazard estimates for the analyzed region. When more data become available, it will be easy to update the GMPEs and recalculate the hazard, leading to increased reliability of the risk estimates for the local building stock.

**Author Contributions:** Conceptualization, B.Đ.B., M.H.-N. and G.P.; methodology, B.Đ.B., M.H.-N. and G.P.; validation B.Đ.B., M.H.-N. and G.P.; formal analysis B.Đ.B., M.H.-N. and G.P.; investigation: B.Đ.B., M.H.-N. and G.P.; resources B.Đ.B., M.H.-N. and G.P.; writing—original draft preparation: B.Đ.B., M.H.-N. and G.P.; final writing—review and editing: B.Đ.B., M.H.-N. and G.P. All authors have read and agreed to the published version of the manuscript.

**Funding:** This research received no external funding.

**Institutional Review Board Statement:** Not applicable.

**Informed Consent Statement:** Not applicable.

**Data Availability Statement:** Not applicable.

**Conflicts of Interest:** The authors declare no conflict of interest.

## Appendix A. The Coefficients Derived in This Study for Scaling Horizontal *PSA*

**Table A1.** Scaling coefficients and standard deviations of the empirical attenuation equations for horizontal *PSA* amplitudes, derived for the region of the north-western Balkans—Equation (1) with  $R$  as the epicentral distance.

$T$	$c_1$	$c_2$	$c_3$	$R_0$	$c_4$	$c_5$	$c_6$	$c_7$	$\sigma_{\log}$
0.050	−0.921	0.352	−1.371	20.3	0.120	−0.058	−0.198	−0.143	0.272
0.075	−0.511	0.337	−1.466	22.1	0.071	−0.032	−0.212	−0.147	0.286
0.100	−0.467	0.360	−1.552	23.5	0.092	−0.003	−0.168	−0.096	0.287
0.150	−0.406	0.396	−1.638	25.8	0.188	0.056	−0.232	−0.188	0.283
0.200	−0.699	0.433	−1.611	24.5	0.256	0.113	−0.203	−0.186	0.290
0.300	−1.643	0.480	−1.391	18.6	0.327	0.203	−0.025	−0.013	0.297
0.400	−2.499	0.540	−1.226	13.8	0.318	0.248	0.100	0.087	0.313
0.500	−2.883	0.579	−1.201	12.3	0.279	0.238	0.134	0.136	0.315
0.750	−3.410	0.596	−1.044	10.9	0.198	0.057	0.066	0.162	0.323
1.000	−3.792	0.604	−0.911	8.9	0.141	−0.098	−0.021	0.129	0.322
1.500	−4.110	0.590	−0.768	8.6	0.077	−0.227	−0.085	0.054	0.323
2.000	−4.295	0.599	−0.825	9.0	0.063	−0.184	−0.077	0.052	0.322

**Table A2.** Scaling coefficients and standard deviations of the empirical attenuation equations for horizontal PSA amplitudes, derived for the region of the north-western Balkans—Equation (1) with  $R$  as the hypocentral distance.

$T$	$c_1$	$c_2$	$c_3$	$R_0$	$c_4$	$c_5$	$c_6$	$c_7$	$\sigma_{\log}$
0.050	−0.503	0.333	−1.513	26.2	0.144	−0.056	−0.174	−0.144	0.279
0.075	−0.042	0.317	−1.626	28.8	0.094	−0.021	−0.189	−0.148	0.293
0.100	0.056	0.340	−1.733	30.7	0.109	0.012	−0.146	−0.095	0.294
0.150	0.245	0.375	−1.875	34.8	0.204	0.075	−0.208	−0.191	0.292
0.200	−0.059	0.413	−1.849	33.0	0.272	0.130	−0.179	−0.191	0.298
0.300	−1.116	0.459	−1.580	25.6	0.355	0.210	0.002	−0.022	0.307
0.400	−2.117	0.516	−1.341	18.1	0.338	0.244	0.124	0.081	0.325
0.500	−2.514	0.552	−1.296	16.1	0.293	0.227	0.154	0.132	0.330
0.750	−3.083	0.569	−1.115	14.5	0.210	0.034	0.081	0.158	0.337
1.000	−3.502	0.578	−0.963	11.7	0.142	−0.109	−0.013	0.127	0.335
1.500	−3.904	0.568	−0.795	10.4	0.083	−0.255	−0.076	0.054	0.332
2.000	−4.063	0.576	−0.862	11.3	0.073	−0.226	−0.067	0.051	0.332

## References

1. Faccioli, E.; Vanini, M. Complex seismic site effects in sediment-filled valleys and implications on design spectra. *Earthq. Eng. Struct. Dyn.* **2003**, *5*, 223–238. [\[CrossRef\]](#)
2. Stamati, O.; Klimis, N.; Lazaridis, T. Evidence of complex site effects and soil nonlinearity numerically estimated by 2D vs1D seismic response analyses in the city of Xanthi. *Soil. Dyn. Earthq. Eng.* **2016**, *87*, 101–115. [\[CrossRef\]](#)
3. Zhu, C.; Chávez-García, F.J.; Thambiratnam, D.; Gallage, C. Quantifying the edge-induced seismic aggravation in shallow basins relative to the 1D SH modelling. *Soil. Dyn. Earthq. Eng.* **2018**, *115*, 402–412. [\[CrossRef\]](#)
4. Ermert, L.; Poggi, V.; Burjanek, J.; Fah, D. Fundamental and higher two-dimensional resonance modes of an Alpine valley. *Geophys. J. Int.* **2014**, *198*, 795–811. [\[CrossRef\]](#)
5. Zhu, C.; Thambiratnam, D. Interaction of geometry and mechanical property of trapezoidal sedimentary basins with incident SH waves. *B Earthq. Eng.* **2016**, *14*, 2977–3002. [\[CrossRef\]](#)
6. Zhu, C.; Thambiratnam, D.; Zhang, J. Response of sedimentary basin to obliquely incident SH waves. *B Earthq. Eng.* **2016**, *14*, 647–671. [\[CrossRef\]](#)
7. Douglas, J. Earthquake ground motion estimation using strong motion records: A review of equations for the estimation of peak ground acceleration and response spectral ordinates. *Earth Sci. Rev.* **2003**, *61*, 43–104. [\[CrossRef\]](#)
8. Peng, Y.; Wang, Z.; Woolery, E.W.; Lyu, Y.; Carpenter, N.S.; Fang, Y.; Huang, S. Ground-motion site effect in the Beijing metropolitan area. *Eng. Geol.* **2020**, *266*, 105395. [\[CrossRef\]](#)
9. Lee, V.W.; Trifunac, M.D.; Bulajić, B.Đ.; Manić, M.I. A preliminary empirical model for frequency-dependent attenuation of Fourier amplitude spectra in Serbia from the Vrancea earthquakes. *Soil Dyn. Earthq. Eng.* **2016**, *83*, 167–179. [\[CrossRef\]](#)
10. Lee, V.W.; Trifunac, M.D.; Bulajić, B.Đ.; Manić, M.I. Preliminary empirical scaling of pseudo relative velocity spectra in Serbia from the Vrancea earthquakes. *Soil Dyn. Earthq. Eng.* **2016**, *86*, 41–54. [\[CrossRef\]](#)
11. Lee, V.W.; Trifunac, M.D.; Bulajić, B.Đ.; Manić, M.I.; Herak, D.; Herak, M.; Dimov, G. Seismic microzoning in Skopje, Macedonia. *Soil Dyn. Earthq. Eng.* **2017**, *98*, 166–182. [\[CrossRef\]](#)
12. Lee, V.W.; Trifunac, M.D.; Bulajić, B.Đ.; Manić, M.I.; Herak, D.; Herak, M.; Dimov, G.; Gičev, V. Seismic microzoning of Štip in Macedonia. *Soil Dyn. Earthq. Eng.* **2017**, *98*, 54–66. [\[CrossRef\]](#)
13. Lee, V.W.; Trifunac, M.D.; Bulajić, B.Đ.; Manić, M.I.; Herak, D.; Herak, M. Seismic microzoning of Belgrade. *Soil Dyn. Earthq. Eng.* **2017**, *97*, 395–412. [\[CrossRef\]](#)
14. Bulajić, B.Đ.; Bajić, S.; Stojnić, N. The effects of geological surroundings on earthquake-induced snow avalanche prone areas in the Kopaonik region. *Cold Reg. Sci. Technol.* **2018**, *149*, 29–45. [\[CrossRef\]](#)
15. Trifunac, M.D.; Brady, A.G. On the correlation of seismic intensity scales with the peaks of recording strong ground motion. *Bull. Seismol. Soc. Am.* **1975**, *65*, 139–162.
16. Eurocode 8: Design of Structures for Earthquake Resistance—Part I: General Rules, Seismic Actions and Rules for Buildings; EC8, EN 1998-1:2004; CEN—European Committee for Standardization: Brussels, Belgium, 2004.
17. Bulajić, B.; Pavić, G.; Hadzima-Nyarko, M. Estimates of PGA values in the horizontal direction for low to medium seismicity regions with deep soil atop deep geological sediments—An example of the city of Osijek, Croatia. *Geomech. Eng.* submitted for publication.
18. Bulajić, B.; Pavić, G.; Hadzima-Nyarko, M. PGA vertical estimates for deep soils and deep geological sediments—A case study of Osijek (Croatia). *Comput. Geosci.* accepted.

19. Bulajić, B.; Hadzima-Nyarko, M.; Pavić, G. Vertical to horizontal strong motion UHS estimates ratios for low to medium seismicity regions with deep soil atop deep geological sediments—An example of the city of Osijek, Croatia. *Appl. Sci.* submitted for publication.
20. Hrvatski zavod za norme: HRN EN 1998-1:2011/NA:2011. *Eurocode 8: Design of Structures for Earthquake Resistance—Part 1: General Rules, Seismic Actions and Rules for Buildings—National Annex*; Hrvatski Zavod za Norme: Zagreb, Croatia, 2011.
21. Lee, V.W. *Influence of Local Soil and Geologic Site Conditions on Pseudo Relative Velocity Spectrum Amplitudes of Recorded Strong Motion Accelerations*; University of Southern California: Los Angeles, CA, USA, 1987.
22. Cipta, A.; Cummins, P.; Irsyam, M.; Hidayati, S. Basin Resonance and Seismic Hazard in Jakarta, Indonesia. *Geosciences* **2018**, *8*, 128. [\[CrossRef\]](#)
23. Seed, H.B.; Ugas, C.; Lysmer, J. Site-dependent spectra for earthquake-resistant design. *Bull. Seismol. Soc. Am.* **1976**, *66*, 221–243.
24. Seed, H.B.; Murarka, R.; Lysmer, J.; Idriss, I.M. Relationships of maximum acceleration, maximum velocity, distance from source, and local site conditions for moderately strong earthquakes. *Bull. Seismol. Soc. Am.* **1976**, *66*, 1323–1342.
25. Stucchi, M.; Rovida, A.; Gomez Capera, A.A.; Alexandre, P.; Camelbeeck, T.; Demircioglu, M.B.; Gasperini, P.; Kouskouna, V.; Musson, R.M.W.; Radulian, M.; et al. The SHARE European Earthquake Catalogue (SHEEC) 1000–1899. *J. Seismol.* **2013**, *17*, 523–544. [\[CrossRef\]](#)
26. Earthquake Catalogue for all Earthquakes with  $M_w \geq 3$  in the Period between 1900 and April 2021 for the Geographic Region between  $41.0^\circ$  N and  $47.0^\circ$  N, and  $12.5^\circ$  E and  $23.0^\circ$  E. United States Geological Survey (USGS), USA. 2021. Available online: <https://earthquake.usgs.gov/earthquakes/search/> (accessed on 23 May 2021).
27. Magaš, N.P.; Mamužić, D.; Matičec, B.; Prtoljan, I.; Galović, M.; Sarkotić Šlat, Ž.; Glovacki, J.; Jagačić, T. *Basic Geological Map of SFRY—Osijek, L34-86*; Socialist Federal Republic of Yugoslavia; Federal Geological Institute: Belgrade, Serbia, 1987.
28. Jordanovski, L.R.; Lee, V.W.; Manić, M.I.; Olumčeva, T.; Sinadnovski, C.; Todorovska, M.I.; Trifunac, M.D. *Strong Earthquake Ground Motion Data in EQINFOS: Yugoslavia. Part I*; Report No. 87-05; Department of Civil Engineering, University of Southern California: Los Angeles, CA, USA, 1987.
29. Ambraseys, N.; Douglas, J.; Margaris, B.; Sigbjörnsson, R.; Smit, P.; Suhadolc, P. Internet site for European strong motion data. In Proceedings of the 12th European Conference on Earthquake Engineering, London, UK, 9–13 September 2002; p. 837.
30. Ambraseys, N.; Douglas, J.; Margaris, B.; Sigbjörnsson, R.; Berge-Thierry, C.; Suhadolc, P.; Costa, G.; Smit, P. Dissemination of European strong-motion data. In Proceedings of the 13th World Conference on Earthquake Engineering, Vancouver, BC, Canada, 1–6 August 2004; Volume 2, p. 32.
31. Accelerograms recorded during March 10, 2010 Peć and November 03, 2010 Kraljevo Earthquakes. Seismological Survey of Serbia, Republic of Serbia. 2021. Available online: <http://www.seismo.gov.rs/O%20zavodu/Infol.htm> (accessed on 21 May 2021).
32. Bulajić, B.Đ.; Manić, M.I.; Ladinović, Đ. Effects of shallow and deep geology on seismic hazard estimates—A case study of pseudo-acceleration response spectra for the north-western Balkans. *Nat. Hazards* **2013**, *69*, 573–588. [\[CrossRef\]](#)
33. Manić, M.I.; Bulajić, B.Đ.; Trifunac, M.D. A note on peak accelerations computed from sliding of objects during the 1969 Banja Luka earthquakes in former Yugoslavia. *Soil Dyn. Earthq. Eng.* **2015**, *77*, 164–176. [\[CrossRef\]](#)
34. Giardini, D.; Woessner, J.; Danciu, L.; Crowley, H.; Cotton, F.; Grünthal, G.; Pinho, R.; Valensise, L. *SHAREConsort. European Seismic Hazard Map for Peak Ground Acceleration, 10% Exceedance Probabilities in 50 Years*; Swiss Seismological Service: Zurich, Switzerland, 2013; ISBN-13 978-92-79-25148-1.
35. Wössner, J.; Laurentiu, D.; Giardini, D.; Crowley, H.; Cotton, F.; Grünthal, G.; Valensise, G.; Arvidsson, R.; Basili, R.; Demircioglu, M.B.; et al. SHARE Consort. The 2013 European Seismic Hazard Model: Key Components and Results. *Bull. Earthq. Eng.* **2015**, *13*, 3553–3596. [\[CrossRef\]](#)
36. Pagani, M.; Garcia-Pelaez, J.; Gee, R.; Johnson, K.; Poggi, V.; Styron, R.; Weatherill, G.; Simionato, M.; Viganò, D.; Danciu, L.; et al. *Global Earthquake Model (GEM) Seismic Hazard Map (Version 2018.1—December 2018)*; GEM Foundation: Pavia, Italy, 2018.
37. Chioccarelli, E.; Cito, P.; Iervolino, I.; Giorgio, M. REASSESS V2.0: Software for single- and multi-site probabilistic seismic hazard analysis. *Bull. Earthq. Eng.* **2019**, *17*, 1769–1793. [\[CrossRef\]](#)
38. Cornell, C.A. Engineering seismic risk analysis. *Bull. Seismol. Soc. Am.* **1968**, *58*, 1583–1606.
39. McGuire, R.K. *Fortran Computer Program for Seismic Risk Analysis*; US Geological Survey Open-File Report 76-77; US Geological Survey: Denver, CO, USA, 1976.
40. Ang, A.H.; Tang, W.H. *Probability Concepts in Engineering: Emphasis on Applications to Civil and Environmental Engineering*; John Wiley Sons: New York, NY, USA, 2006.
41. Bazzurro, P.; Cornell, C.A. Disaggregation of seismic hazard. *Bull. Seismol. Soc. Am.* **1999**, *89*, 501–520.
42. McGuire, R.K. Probabilistic seismic hazard analysis and design earthquakes: Closing the loop. *Bull. Seismol. Soc. Am.* **1995**, *85*, 1275–1284.
43. Pavić, G.; Hadzima-Nyarko, M.; Bulajić, B. A Contribution to a UHS-based Seismic Risk Assessment in Croatia—A Case Study for the City of Osijek. *Sustainability* **2020**, *12*, 1796. [\[CrossRef\]](#)
44. Pavić, G.; Hadzima-Nyarko, M.; Bulajić, B.; Jurković, Ž. Development of Seismic Vulnerability and Exposure Models—A Case Study of Croatia. *Sustainability* **2020**, *12*, 973. [\[CrossRef\]](#)
45. Ruan, B.; Zhao, K.; Wang, S.-Y.; Chen, G.-X.; Wang, H.-Y. Numerical modeling of seismic site effects in a shallow estuarine bay (Suai Bay, Shantou, China). *Eng. Geol.* **2019**, *260*, 105233. [\[CrossRef\]](#)

- 
46. Derras, B.; Bard, P.-Y.; Régnier, J.; Cadet, H. Non-linear modulation of site response: Sensitivity to various surface ground-motion intensity measures and site-condition proxies using a neural network approach. *Eng. Geol.* **2020**, *269*, 105500. [[CrossRef](#)]
  47. Bijelić, N.; Lin, T.; Deierlein, G. Quantification of the influence of deep basin effects on structural collapse using SCEC CyberShake earthquake ground motion simulations. *Earthq. Spectra* **2019**, *35*, 1845–1864. [[CrossRef](#)]